

AN ANALYSIS OF DISPLACEMENT MEASUREMENTS FOR LISBON, PORTUGAL, USING COMBINED INSAR AND GNSS DATA

D. Roque⁽¹⁾, E. Simonetto⁽²⁾, A.P. Falcão⁽³⁾, D. Perissin⁽⁴⁾, F. Durand⁽²⁾, L. Morel⁽²⁾, A.M. Fonseca⁽¹⁾, L. Polidori⁽²⁾

⁽¹⁾ *Laboratório Nacional de Engenharia Civil, Avenida do Brasil 101 Lisboa Portugal, Email: droque@lnec.pt; anafonseca@lnec.pt*

⁽²⁾ *École Supérieure des Géomètres et Topographes, 1 Boulevard Pythagore Campus Universitaire 72000 Le Mans France, Email: elisabeth.simonetto@esgt.cnam.fr; frederic.durand@esgt.cnam.fr; laurent.morel@cnam.fr; laurent.polidori@esgt.cnam.fr*

⁽³⁾ *Instituto Superior Técnico – Universidade de Lisboa, Avenida Rovisco Pais 1 1049-001 Lisboa Portugal, Email: ana.p.falcao@tecnico.ulisboa.pt*

⁽⁴⁾ *Purdue University, 610 Purdue Mall West Lafayette IN47907 USA, Email: perissin@purdue.edu*

ABSTRACT

Atmospheric effects are still a limitation to the application of InSAR techniques for displacement measurement. In this study, zenith total delay (ZTD) values derived from global navigation satellite system (GNSS) are used to correct interferograms from tropospheric effects. Displacement measurements are obtained from the corrected interferograms through a persistent scatterer interferometry approach. The influence of different interpolation methods on the construction of ZTD maps is tested through two different algorithms: cubic spline and ordinary kriging. Differences are observed between the cumulative displacement maps obtained with both interpolators, but atmospheric effects are still present, possibly due to the small number of available GNSS stations.

1. INTRODUCTION

Interferometric synthetic aperture radar (InSAR) is a technique that enables displacement measurements at the Earth surface. Atmospheric effects have been a hindrance for displacement computation through differential InSAR (DInSAR) techniques. In order to overcome this limitation, some authors have proposed the estimation of atmospheric delays through other methods, such as weather models [1], [2] and global navigation satellite system (GNSS) [3], [4], [5]. In this study, the authors intend to compare atmospheric effects obtained from GNSS observations with those achieved through persistent scatterers interferometry (PSI). The paper presents a method to calculate the tropospheric delay from GNSS data, in which zenith total delay (ZTD) values are converted into differential tropospheric phase (DTP) in SAR geometry and then removed from the interferograms used for the displacement analysis. An application of this method has been presented in [6], where troposphere-corrected interferograms were used to study the behaviour of the Piton de la Fournaise volcano, in La Réunion, France. In the present study, two interpolators are tested in order to acquire GNSS-derived ZTD values for each persistent

scatterer (PS) location: cubic spline and ordinary kriging.

The proposed method is applied to the city of Lisbon, Portugal, which has been hit by catastrophic events in the past, such as earthquakes and tsunamis. Also, the geological properties of its location and the proximity to the Tagus River turn it into a city prone to ground instability.

2. STUDY AREA AND DATASET

The region of interest has an area of, approximately, 255 km² and includes the city of Lisbon and its neighbourhood (Fig. 1).

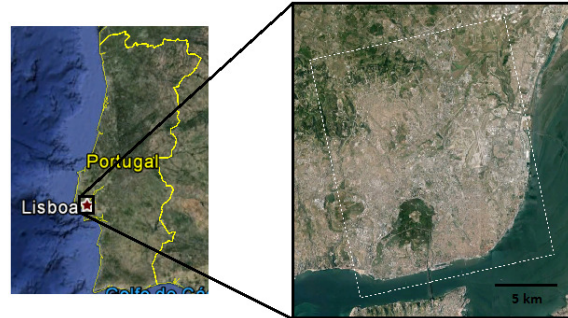


Figure 1. Location of the study area.

A dataset of 8 Envisat ASAR images, acquired between September 2008 and October 2009, during an ascending pass and with VV polarization were considered (Tab. 1).

Table 1. Acquisition days of ASAR images.

Acquisition date	Orbit
2008/09/14	34209
2008/12/28	35712
2009/04/12	37215
2009/05/17	37716
2009/06/21	38217
2009/07/26	38718
2009/08/30	39219
2009/10/04	39720

Portugal has two networks of GNSS permanent stations: the network SERVIR, belonging to the Centre of Geospatial Information of the Army, and ReNEP, of the General-Directorate of the Territory. Both networks are operating since 2006. A total of 10 stations with data collected during the time interval of the ASAR images acquisition were identified inside the footprints of the images. The area covered by the GNSS stations contains the study area.

The PSI processing was performed with SARPROZ® software [7] and the GNSS data was processed with GAMIT. The conversion from ZTD to DTP was made with MATLAB®. The interpolation was performed with the spatial analyst extension of ArcGIS® and the analysis of the obtained results with ENVI® software. Altitude information was provided by the SRTM digital elevation model (DEM), with 90 m of spatial resolution.

3. METHODS

For the GNSS processing, hourly RINEX files are available for the 10 permanent stations, which were merged into daily files. In a first step, the coordinates of the stations were computed with high precision in the reference frame ITRF2008 for the central epoch of the considered time interval. Then, the ZTD values were calculated for each GNSS station and for each date of the ASAR images. The coordinates of the stations were converted into WGS84.

For the interpolation of the ZTD values, two techniques were used: cubic spline and ordinary kriging. It was verified that a minimum of eight stations is required to assure a good performance of the kriging interpolator. Therefore, as at the time the study was performed there were less than eight processed stations for the dates 2008/09/14 and 2009/04/12, these images were removed from the analysis. Six interpolated ZTD maps were built for each interpolator, with a pixel spacing of 20 m.

ZTD is composed of a hydrostatic and of a wet component and provides the delay of the signal caused by troposphere at the zenith of each permanent station. Slant Total Delay (STD) can be computed from the two components of ZTD through Eq. 1

$$STD = ZHD \cdot mf_H(el) + ZWD \cdot mf_W(el) \quad (1)$$

where ZHD and ZWD are the hydrostatic and wet components of ZTD, respectively, and mf_H and mf_W are the corresponding mapping functions, which map the delays to a certain elevation angle el . ZHD and the mapping functions are modelled, while ZWD has to be estimated. As for the mapping functions, Eq. 2 is used to project the observations from the zenith direction into the ASAR sensor line of sight (LOS), where el is the elevation angle of the sensor.

$$mf(el) = \frac{1}{\sin(el)} \quad (2)$$

The computed STD is then converted to unwrapped tropospheric phase delay (ϕ_{tropo}) through Eq. 3.

$$\phi_{tropo} = \frac{4\pi}{\lambda} STD \quad (3)$$

Using orbital information (satellite location and velocity), SAR sensor properties and image acquisition time, the tropospheric phase delay is used to compute the atmospheric phase screen (APS) for each image acquisition time. The difference of APS maps between two epochs (corresponding to the epochs considered in the interferograms from the PSI processing) is calculated and corresponds to the unwrapped DTP. After being wrapped, the achieved DTP is removed from the differential interferograms.

For the PSI processing, a master image is selected in order to minimize both perpendicular and temporal baselines – 2009/05/17. The whole dataset is coregistered based on orbital information and it is georeferenced through the manual selection of a ground control point. Differential interferograms are built by computing the phase difference between each slave and the master and by removing the phase component corresponding to the DEM. After the removal of wrapped DTP, the PSI processing is performed over the corrected interferograms and a LOS displacement map is obtained. The whole workflow is presented in Fig. 2.

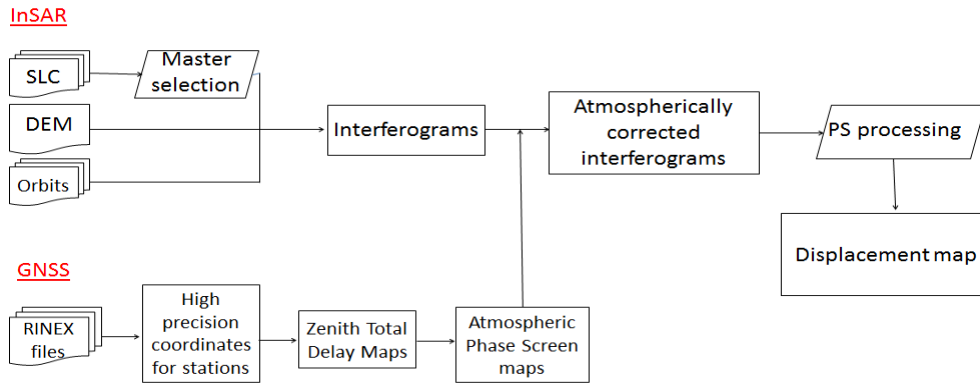


Figure 2. Workflow of the processing.

4. RESULTS

The available GNSS stations occupy an area of, approximately, 4000 km², which contains the study area of the project. A minimum of 8 and a maximum of 10 stations were used for each date. Both interpolators enabled the construction of continuous ZTD maps (Fig. 3). The ZTD values vary between 2.3 m and 2.6 m. The highest values are observed at 2009/10/04 and the lowest at 2008/12/28.

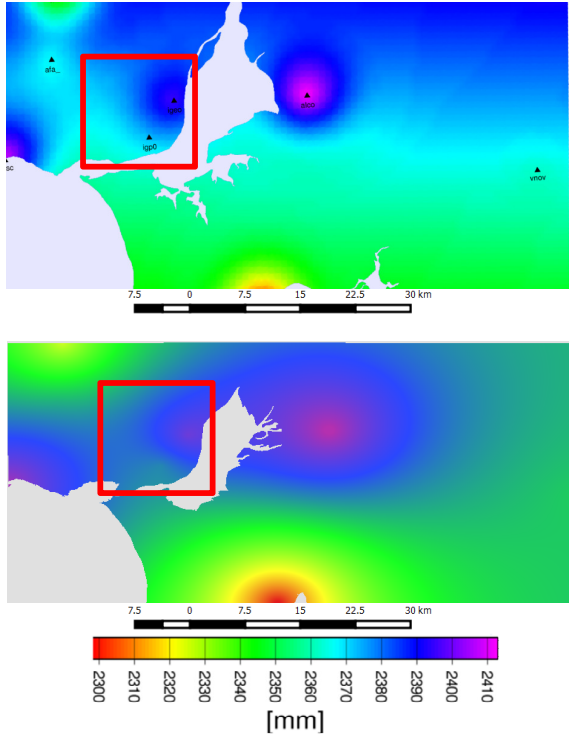


Figure 3. Interpolated ZTD maps for 2008/12/28: cubic spline (top) and ordinary kriging (bottom); study area inside red square.

Although the number of available GNSS stations is enough to build the interpolation maps, there are only three stations inside the study area. As the remaining ones are located some tens of kilometres away from the region of interest, they have little influence on the results.

The original interferograms are noisy and some of them present a fringe pattern. The perpendicular baselines for each interferogram are presented at Tab. 2.

Table 2. Perpendicular baselines.

Interferogram	Perpendicular baseline (m)
2008/12/28 – 2009/05/17	26.7
2009/06/21 – 2009/05/17	-224.5
2009/07/26 – 2009/05/17	184.7
2009/08/30 – 2009/05/17	217.9
2009/10/04 – 2009/05/17	-257.9

Fig.4 presents the interferogram formed by the image pair 2008/12/28 – 2009/05/17, which is the one with the smallest perpendicular baseline. Before the troposphere correction (Fig. 4 top), a fringe and noise are visible, which are no longer present at the corrected interferogram (Fig. 4 bottom). Instead, the last image shows a spatial pattern (identified with the red arrow) which is consistent with displacement observed at the study area in a previous study [8].

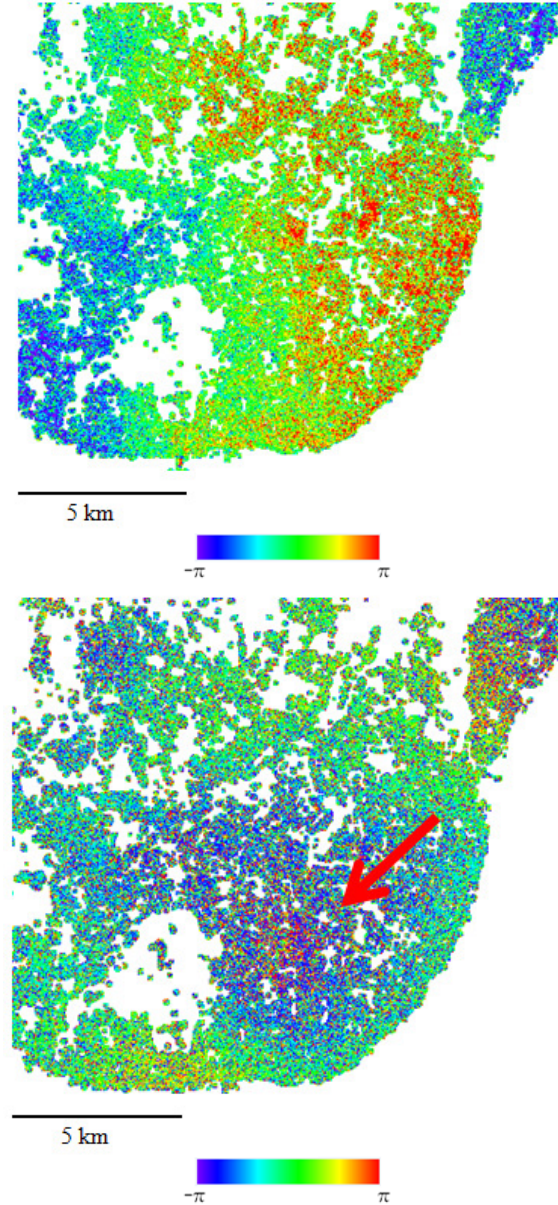


Figure 4. Original (top) and troposphere-corrected (bottom) interferograms (interpolation method: cubic spline).

Two cumulative displacement maps were obtained from the corrected interferograms: one corresponding to the cubic spline and the other one to the ordinary kriging

interpolated ZTD values (Fig. 5).

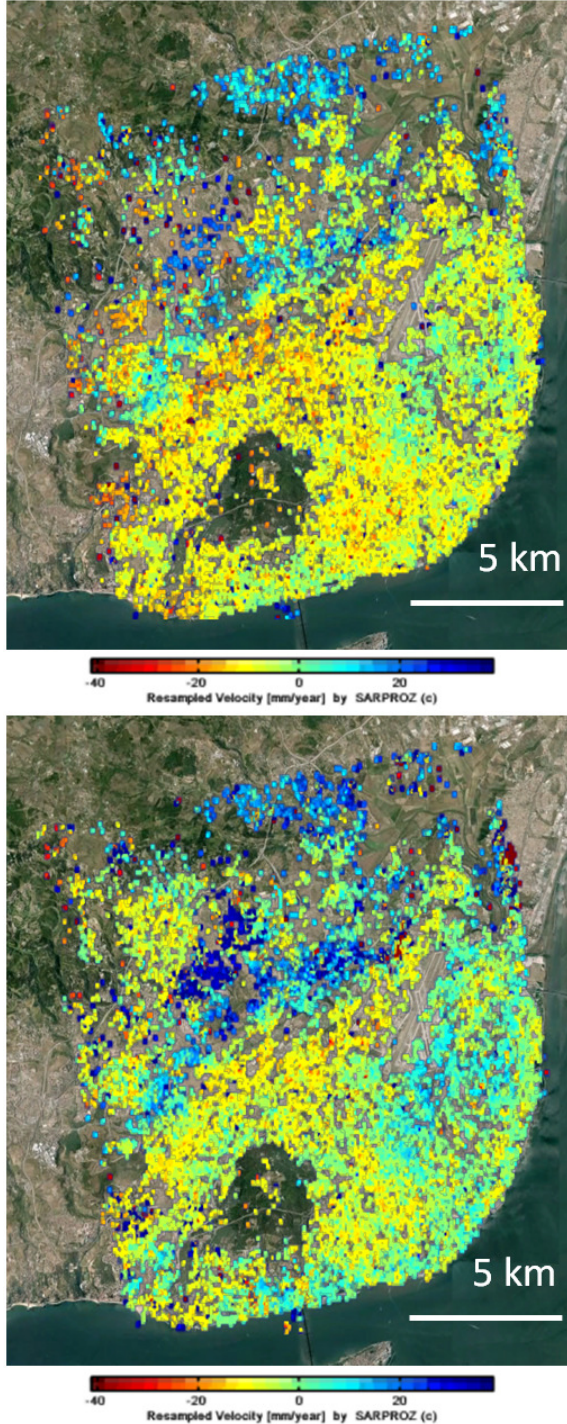


Figure 5. Cumulative displacement maps corresponding to cubic spline (top) and ordinary kriging (bottom).

The cumulative displacement maps were built using a linear displacement model for the PSI processing. Only scatterers presenting a temporal coherence above 0.9 were considered to be PS. A density of 53 PS/km² was

obtained for both approaches.

Some differences are observed when visually comparing both cumulative displacement maps. The map corresponding to cubic spline presents a larger area moving away from the sensor, while the one built through ordinary kriging shows a stronger movement towards the sensor.

For a quantitative comparison, statistics of the cumulative displacement maps were computed. Besides, a PSI processing was performed on the non-corrected interferograms and a cumulative displacement map was obtained, whose statistics were also evaluated (Tab. 3).

Table 3. Statistics for the cumulative displacement maps obtained with corrected and non-corrected interferograms.

	Min (mm)	Max (mm)	Average (mm)	Standard Deviation (mm)
Cubic Spline	-40.9	42.1	-0.46	4.22
Ordinary Kriging	-29.8	30.3	0.79	4.31
Not corrected	-30.2	30.5	1.18	5.45

It is observed that cubic spline method led to more extreme values of cumulative displacement than the approach using ordinary kriging. Ordinary kriging results are the most similar to those obtained from uncorrected interferograms, as both extreme and average values are similar for both cases. Although average values are different for cubic spline and ordinary kriging corresponding displacement maps, their standard deviations are close.

None of the cumulative displacement maps obtained through the corrected interferograms shows spatial patterns consistent with known displacement at the study area during the considered time interval. Therefore, the results for both interpolators may still be affected by atmospheric effects.

5. CONCLUSIONS

This study proposes a method to estimate the tropospheric contribution to APS from GNSS-derived ZTD data. Cubic spline and ordinary kriging enable the interpolation of ZTD values for each PS location, which are then used to compute differential tropospheric phase. Cumulative displacement maps are built, through PSI processing, from interferograms corrected of the differential tropospheric phase.

It was verified that the results depend on the number and spatial distribution of the GNSS stations and also of the interpolation technique used to compute the ZTD maps.

The obtained cumulative displacement maps are still affected by atmospheric effects, maybe due to the small

number of GNSS stations inside the study area (only three). Therefore, it is not possible to perform a geophysical analysis of the displacements in the city of Lisbon from the obtained results. The authors intend to improve the present work by: i) increasing the number of GNSS stations and the ASAR image dataset; ii) testing other interpolation techniques; iii) comparing the LOS cumulative displacements obtained from this technique with those derived from the traditional PSI approach.

ACKNOWLEDGEMENTS

The authors would like to thank ESA for providing the Envisat ASAR images through ESA CAT-1 9366. They would also like to thank the Portuguese General-Directorate of the Territory and the Centre for Geospatial Information of the Army for providing the GNSS data. This work is partially funded by the French Space Agency CNES (TOSCA 2014 and 2015 programs).

6. REFERENCES

1. Jung, J., Kim, D. J., & Park, S. E. (2014). Correction of atmospheric phase screen in time series InSAR using WRF model for monitoring volcanic activities. *Geoscience and Remote Sensing, IEEE Transactions on*, **52**(5), 2678-2689
2. Jolivet, R., Grandin, R., Lasserre, C., Doin, M. P., & Peltzer, G. (2011). Systematic InSAR tropospheric phase delay corrections from global meteorological reanalysis data. *Geophysical Research Letters*, **38**(17), L17311, doi:10.1029/2011GL048757
3. Li, Z., Muller, J. P., Cross, P., & Fielding, E. J. (2005). Interferometric synthetic aperture radar (InSAR) atmospheric correction: GPS, Moderate Resolution Imaging Spectroradiometer (MODIS), and InSAR integration. *Journal of Geophysical Research: Solid Earth*, **110**(B3)
4. Li, Z., Fielding, E. J., Cross, P., & Muller, J. P. (2006). Interferometric synthetic aperture radar atmospheric correction: GPS topography-dependent turbulence model. *Journal of Geophysical Research: Solid Earth*, **111**(B2)
5. Cheng, S., Perissin, D., Lin, H., & Chen, F. (2012). Atmospheric delay analysis from GPS meteorology and InSAR APS. *Journal of Atmospheric and Solar-Terrestrial Physics*, **86**, 71-82
6. Simonetto, E., Durand, F., Morel, L., El Hamri, Y., Froger, J. L., Nicolas, J., Durand, S. & Polidori, L. (2015). Influence of GNSS Configuration and Map Interpolation Method on InSAR Atmospheric Phase Assessment. In *ESA Special Publication* (Vol. 731, p.32)
7. Perissin, D. (2016). SARPROZ Manual. Available at <http://www.sarproz.com/software-manual/>, last accessed in May 2016.
8. Heleno, S. I., Oliveira, L. G., Henriques, M. J., Falcão, A. P., Lima, J. N., Cooksley, G., Ferretti, A., Fonseca, A.M., Lobo-Ferreira, J.P. & Fonseca, J. F. (2011). Persistent scatterers interferometry detects and measures ground subsidence in Lisbon. *Remote Sensing of Environment*, **115**(8), 2152-2167.